DOI: 10.1002/chem.200701831

Coupling Sol–Gel Synthesis and Microwave-Assisted Techniques: A New Route from Amorphous to Crystalline High-Surface-Area Aluminium Fluoride

Damien Dambournet,[a] Gehan Eltanamy,[c] Alexandre Vimont,[b] Jean-Claude Lavalley,[b] Jean-Michel Goupil,[b] Alain Demourgues,[a] Etienne Durand,[a] Jérôme Majimel,[a] Stephan Rudiger,[c] Erhard Kemnitz,*[c] John M. Winfield,[d] and Alain Tressaud*[a]

Abstract: A non-aqueous sol–gel Al-based fluoride has been subjected to the microwave solvothermal process. The final material depends on the temperature heat treatment used. Three types of material have been prepared: 1) for low temperature heat treatment (90 °C) X-ray amorphous alkoxy fluoride was obtained; 2) for the highest temperature used (200 °C) the metastable form β-AlF_3 was obtained with a very large surface area of 125 $m^2 g^{-1}$. The mechanism of the amorphous⇄crystalline transformation has been rationalised by the occurrence of a decomposition reaction of the gel fluoride induced by the microwave irradiation. 3) Finally, at intermediate temperature (180 °C) a multi-component material mixture exhibiting a huge surface area of 525 $m^2 g^{-1}$ has been obtained and further investigated after mild post-treatment fluorination using F_2 gas. The resulting aluminium-based fluoride still possesses a high-surface-area of 330 $m^2 g^{-1}$. HRTEM revealed that the solid is built from large particles (50 nm) identified as α-AlF_3, and small ones (10 nm), relative to an unidentified phase. This new high-surface-area material exhibits strong Lewis acidity as revealed by pyridine adsorption and catalytic tests. By comparison with other materials, it has been shown that whatever the composition/structure of the Al-based fluoride materials, the number of strong Lewis acid sites is related to the surface area, highlighting the role of surface reconstruction occurring on a nanoscopic scale on the formation of the strongest Lewis acid sites.

Keywords: fluorides · high surface area · Lewis acids · microwave solvothermal processes · nanostructures · sol–gel processes

Introduction

A non-aqueous sol–gel process has been reported by Kemnitz et al.[1] for the preparation of X-ray-amorphous metal fluorides with high-surface-area and exhibiting very strong Lewis acidity. In the first step, an incomplete reaction between a metal alkoxide and hydrofluoric acid takes place in an organic solvent: $M(OR)_3 + x\,HF \rightarrow MF_x(OR)_{3-x} + x\,ROH$. Whereas the formation of the M–F bond is thermodynamically favoured when compared to the M–OR bond, the formation of a gel limits the OR/F substitution. After drying this gel by heating up to 70 °C, a powdered metal alkoxy fluoride, named dry gel, with the general formula $MF_x(OR)_{3-x}\cdot y\,ROH$ can be obtained. In a second step, a post-fluorination treatment, using gaseous CFCs or anhydrous HF, is performed to replace the remaining alkoxy groups by fluoride anions and to obtain pure high-surface-area aluminium fluoride (HS-AlF_3).

[a] D. Dambournet, Dr. A. Demourgues, E. Durand, Dr. J. Majimel, Dr. A. Tressaud
Institut de Chimie de la Matière Condensée de Bordeaux-CNRS
Université Bordeaux 1, 87, Avenue du Dr. A. Schweitzer
33608 Pessac cedex (France)
Fax: (+33) 540-002-761
E-mail: tressaud@icmcb-bordeaux.cnrs.fr

[b] Dr. A. Vimont, Prof. J.-C. Lavalley, Prof. J.-M. Goupil
Laboratoire Catalyse et Spectrochimie
UMR 6506, CNRS-ENSICAEN-Université de CAEN
Boulevard du Maréchal Juin, 14050 Caen Cedex (France)

[c] G. Eltanamy, Dr. S. Rudiger, Prof. Dr. E. Kemnitz
Institut für Chemie, Humboldt-Universität zu Berlin
Brook-Taylor-Strasse 2, 12489 Berlin (Germany)
Fax: (+49) 30-20937277
E-mail: erhard.kemnitz@chemie.hu-berlin.de

[d] Prof. J. M. Winfield
Department of Chemistry, University of Glasgow
Glasgow G12 8QQ, Scotland (UK)

At every step, those parameters which could have an influence on the properties of HS-AlF_3 have been fully investigated regarding the surface area and the reactivity properties of the final solid.[2] Concerning the liquid-phase fluorination step, the authors have pointed out a minor effect on the final solid properties of parameters such as the sol–gel synthesis temperature, the concentration, and even the nature of the alkoxide.

On the other hand, due to the peculiar heating mode[3] resulting from the interaction between the material and the electric field component, microwave-assisted synthesis has proved to be a promising new technique.[4] Recently, this microwave-assisted solvothermal route was successfully applied to the synthesis of nanosized, crystalline aluminium hydroxy fluorides.[5]

The present work deals with the transformation under microwave heating of a fluoride gel obtained through the sol–gel process previously described. The influence of the temperature heat treatment on the final product will be discussed. In addition, the morphology and some catalytic properties of a high-surface-area aluminium fluoride obtained by fluorination of the dry gel using F_2 gas is reported. (Herein, for the sake of simplicity the material is quoted as "aluminium fluoride" even if it contains traces of hydroxyls).

Experimental Section

Synthesis procedure: A wet gel, obtained by reacting aluminium isopropoxide dissolved in isopropanol with an anhydrous HF/diethyl ether mixture in the molar concentration ratio $C_{HF}/C_{Al}=3$, was used as the starting precursor. Syntheses were conducted inside a microwave digestion system (MARS 5, CEM Corporation). The microwave procedure consisted of two steps, both in the same system: a heat treatment and a drying step. The heat treatment was performed in solvothermal conditions, that is, in a closed system, for one hour. The gel (50 mL) was enclosed in a PTFE container. The temperature was monitored by an optical fibre and was regulated by percent increments of the microwave power (300 W, 2.45 GHz frequency). Four different temperatures were used: 90, 130, 180, and 200 °C. The internal pressure was measured by a pressure sensor. After the heat treatment, the gel was allowed to cool down to room temperature prior to the drying step. Such a second microwave treatment was performed at $T=90$ °C by using a specific device in which solvents were evaporated through primary vacuum and argon flow. It should be noted that there is no modification induced on the final compound by the drying conditions. To ascertain this, various drying temperatures were used ($50<T<150$ °C) and no influence on the final state of the compound was observed. In the present work, only the influence of the heat treatment parameters on the final compound properties will be discussed. Finally, the obtained dry gel, a white powder, was outgassed in a conventional oven at 200 °C for 4 h under primary vacuum.

Characterisations

X-ray diffraction analysis: Powder X-ray diffraction patterns were recorded on a Philips PW1820, PANalytical X'Pert diffractometer in a Bragg-Brentano geometry (θ-2θ), using $Cu_{K\alpha1/\alpha2}$ radiation ($\lambda=1.54051$ Å).

Textural measurements: N_2 adsorption isotherms were recorded at 77 K on an ASAP 2000 instrument from Micromeritics. The powder sample (~200 mg) was evacuated overnight at 473 K under 0.1 Pa pressure, prior to N_2 adsorption. The total pore volume, V_{pore}, was calculated from the volume of nitrogen adsorbed at relative pressure $P/P°=0.99$. The apparent specific surface area, S_{BET}, was calculated from the BET method applied in the $P/P°$ range between 0.03 and 0.25. The pore size distribution was obtained taking the Barrett–Joyner–Halenda (BJH) algorithm using the adsorption branch. In Table 1, the mesopore size was taken as the value at the "top" of the ($dV/d\log D$) plot, in which D is the pore diameter.

Table 1. Porosity measurements by N_2 isotherm results.

Heating temperature [°C]	V_{pore} [mL g^{-1}]	S_{BET} [m^2 g^{-1}]	Pore size [nm]
90	0.43	425	4.1
130	0.62	470	5.3
180	0.76	525	7.4
200	0.77	125	≈50

Post-fluorination treatment: The sample was placed in a Ni crucible and was outgassed at 80 °C for 1 h. Undiluted F_2 gas was introduced with a flow of 10 mL min^{-1}. The temperature was increased to 225 °C and maintained for 5 h. At the end of the experiment, unreacted F_2 gas was eliminated from the oven by a N_2 flow and reacted on soda lime. *High Resolution Transmission Electron Microscopy (HRTEM)*: HRTEM was performed on TECNAI F20 equipment with a field emissive gun, operating at 200 kV and with a point resolution of 0.24 nm. TEM samples were prepared by dispersing a few milligrams of powder in isopropanol. The dispersion was then immersed for ten minutes in an ultrasonic bath in order to disagglomerate the powder particles. Finally, one drop was deposited on a Formvar/carbon copper grid.

FT-IR spectroscopy: Approximately 20 mg of powder was pressed into a self-supported disc (2 cm^2 area). Transmission IR spectra were recorded in the 500–5600 cm^{-1} range with a 4 cm^{-1} resolution on a Nicolet Nexus spectrometer. The cell was connected to a vacuum line for the evacuation and activation steps. Samples were activated at 300 °C for 4 h under vacuum.

After activation, the acidity of the material was studied by IR spectroscopy, with adsorbed pyridine as a spectroscopic probe. Pyridine (Aldrich, 99+ % grade) was dried on molecular sieves prior to use. Introduction of pyridine was performed at equilibrium pressure (133 Pa) and then evacuated under vacuum at increasing temperatures to remove physisorbed species.

Catalytic tests: Dismutation of $CHClF_2$ was performed in a continuous-flow fixed-bed reactor. A mixture of $CHClF_2$:N_2 (5:20 mL min^{-1}) was passed through the sample. The temperature was increased stepwise and held at each respective temperature for 20 min. After reaching 99 % conversion, the reactor was cooled down to 50 °C.

The isomerisation of 1,2-dibromohexafluoropropane $CBrF_2CBrFCF_3$ was tested at room temperature. Inside a glove box, the sample (20 mg) was placed in a flask equipped with a magnetic stirrer. The flask was then sealed with a rubber septum cap. $CBrF_2CBrFCF_3$ (~300 μL) was added through the septum by using a μL syringe and the mixture was stirred at ambient temperature for 2 h. The yield of the target product was deduced by ^{19}F NMR spectroscopy (solvent: $CDCl_3$).

Elemental analysis: Fluorine and aluminium contents were quantified by the Service Central of Analysis (SCA-CNRS, Vernaison): F titration with a specific electrode and Al by ICPMS. The carbon content was determined by the combustion method using LECO CHNS-932 apparatus.

Results and Discussion

Microwave-assisted synthesis

Synthesis features and characterisation of the dry gel: During the solvothermal step, the synthesis temperature was tuned at four levels: 90, 130, 180, and 200 °C. Table 2 summarises the internal pressure measured during the heat treatment.

Table 2. Experimental parameters of the microwave process. The reported chamber pressure was measured before the end of the heat treatment. The appearance of gel was noted after cooling down to room temperature.

Heating temperature (°C)	Chamber pressure (bars)	Appearance after solvothermal treatment	Final F/Al molar ratio of the dry gel	Weight loss (%) of the dry gel at 200°C
90	<1	Gel	1.5	50
130	4–5	viscous gel	1.7	42
180	16–18	viscous gel	2 (C: 12 wt%)	26
200	48–51	liquid	2.7 (C: 0.1 wt%)	5

The state of the gel observed after the corresponding treatment is also noted. Based on these observations, it is clear that the synthesis temperature is a crucial parameter. Whereas at temperatures below 200°C the gel state remains, for $T=200$°C a liquid is obtained after reaction, which is in contrast with the initial gel state of the starting material. It should be noted that a high pressure is measured under the latter conditions (see Table 2).

After the final microwave-assisted drying, the nature of the obtained solid depends on the synthesis temperature. From the powder X-ray diffraction patterns displayed in Figure 1, three steps can be distinguished. At 90 and 130°C, X-ray amorphous materials are obtained. At 180°C the crystallisation has started, as revealed by two well-defined X-ray lines at approximately $2\theta=25$ and 51°, which are related to the main lines of the thermodynamically stable α-AlF_3 phase.[6] Several additional broad X-ray peaks, located at 4.7 and 3.1 Å and marked by asterisks in Figure 1, were detected, but no satisfactory indexing could be found using the JCPDS data files. A derived rutile aluminium oxy fluoride has been reported[7] and the main X-ray peak of this phase is close to the peak detected at 3.1 Å. These peaks present large full width at half maximum (FWHM) values compared to those of α-AlF_3, suggesting that this unknown phase consists of smaller particles. Finally, when the reaction temperature is 200°C, a very crystalline aluminium fluoride is formed that exhibits the hexagonal tungsten bronze type structure, that is, β-AlF_3.[8]

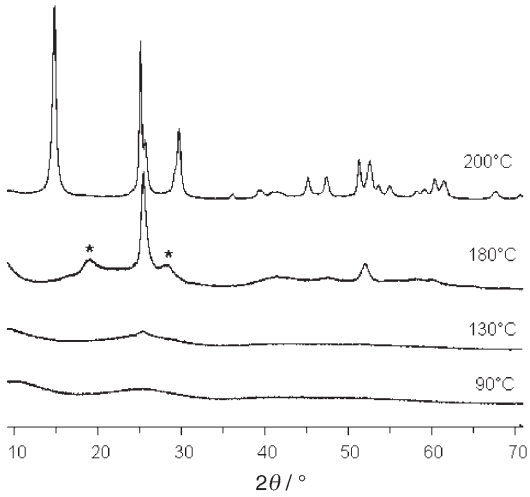

Figure 1. X-ray diffraction powder patterns of samples obtained after microwave irradiation at various temperatures (* refers to an unknown phase).

This evolution of the crystalline features can be related to the increase of the F/Al molar ratio, as displayed in Table 2. A slight increase of the fluorine content from 1.5 to 1.7 is observed when the heat treatment temperature is increased from 90 to 130°C. Treatments at higher temperature greatly improve the fluorine content. Moreover, the F/Al molar ratio increases sharply from 2 to 2.7 when the temperature is increased from 180 to 200°C. In addition, the content of organic moieties can be basically quantified by measuring the weight loss after outgassing at 200°C under dynamic vacuum (Table 2). A general trend can be observed: the higher the fluorine content, the lower the weight loss and the lower the organic content. For dry gels obtained at high temperatures (180 and 200°C), the carbon contents were measured to be 12.7 and below 0.1 wt%, respectively. Such results imply the formation of intermediate alkoxy fluorides with the already reported general formula AlF_{3-x}-$(OiPr)_x \cdot y\,i$PrOH[9] when the synthesis was conducted below 200°C. The 0.1 wt% C content is clear evidence that the phase obtained at 200°C is no longer an alkoxy fluoride, but is more likely to be an oxy or hydroxy fluoride.

Concerning the textural properties of the obtained dry gels, the nitrogen adsorption–desorption isotherms, as well as the derived pore size distribution, are collected in Figure 2A. The BET specific surface area, total pore volume, and mesopore size are listed in Table 1.

The most salient observation is the very large surface area of the obtained materials. As far as the textural properties are concerned, a clear distinction can be made between the sample prepared at 200°C and those obtained at lower temperatures. Samples prepared below 200°C are mesoporous materials exhibiting a type IV isotherm with a well-defined plateau and an H2-type (IUPAC) hysteresis loop. When the treatment temperature is raised from 90 to 180°C, the total pore volume increases from 0.43 to 0.76 mL g^{-1}, whereas the surface area only increases from 425 to 525 $m^2 g^{-1}$. This is ascribed to an enlarging of the width of the mesopores, which is directly confirmed by a shift of the hysteresis loop toward higher relative pressures. The mesoporous network could be described by a distribution of mesopores centred at increasing width, from 3.7 to 6.3 nm (Figure 2B).

The sample prepared at 200°C also exhibits a type IV isotherm, but with a very different shape and an H1-type loop observed at high relative pressures (above ≈ 0.95). So it can be observed in Figure 2B that this material exhibits a very broad distribution of wide pores. The decrease of the surface area down to 125 $m^2 g^{-1}$ while a high pore volume is preserved (0.77 mL g^{-1}) is consistent with the completion of a

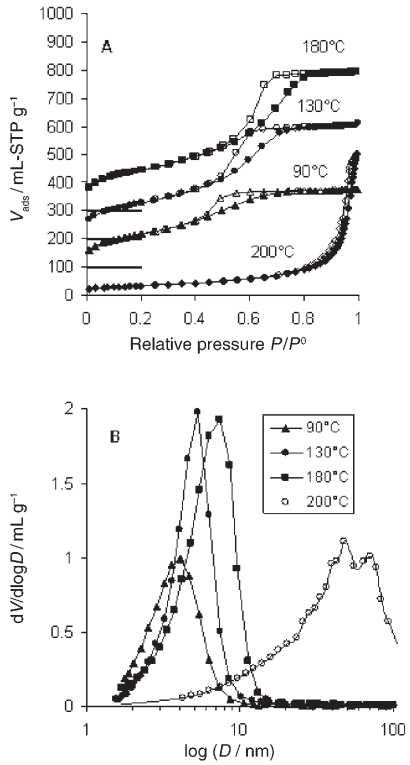

Figure 2. A) N_2 adsorption isotherms of materials prepared at various temperatures. Filled symbols correspond to the adsorption branch and empty symbols to the desorption branch. For the sake of readability the isotherms are shifted upwards for $n \times 100\,mL\,g^{-1}$. B) Pore size distribution.

crystallisation process, in agreement with the very well crystallised state of this material.

From amorphous to crystalline materials—proposed mechanisms: Based on the above results, it appears that the temperature at which the microwave treatment is performed is the main factor that drives the nature of the final product. However, the temperature factor seems to induce a complex mechanism involving the different constituents of the mixture, and this point will be discussed below.

At 90 and 130 °C, the fluorination of the alkoxide remains very low and the resulting aluminium alkoxy fluoride is X-ray amorphous due to the presence of a large number of organic moieties, which limit the coherence length of the crystallites. At these temperatures, the dry gel should exhibit the topology of the original gel, which consists of an $Al(F,OR)_3$ network. An increase of the synthesis temperature up to 180 °C favours the formation of higher fluorinated species, as revealed by the increase of the F/Al molar ratio up to 2 (Table 2). This increase in fluorine content is simultaneous with the appearance of crystalline domains, most of them being the α-AlF_3. The appearance of this phase within an amorphous matrix reveals the inhomogeneity of the activated gel mixture. Such inhomogeneities have also been demonstrated by ^{27}Al NMR spectroscopy on the dry gel prepared with a low C_{HF}/C_{Al} molar ratio ($R=2$). Aluminium species with various anionic environments,[2] that is, fluorinated species located at −10 ppm and oxygenated species at 14 ppm, are highlighted. Regarding the rather low FWHM for the X-ray peaks of the α-AlF_3 phase obtained at 180 °C (Figure 1), it is clear that this phase consists of large particles relative to the other constituents. The other constituents of this sample should be considered as an $AlF_{3-x}(OiPr)_x$ and/or an Al oxy fluoride phase with very small particle size giving rise to the extremely high-surface-area (525 $m^2\,g^{-1}$).

The crystallisation process begins between 130 and 180 °C and induces an increase of the kinetics of fluorination and, surprisingly, an increase of the surface area. It can be suggested that the densification of α-AlF_3 particles implies a migration of matter which results in a high improvement of the porous volume associated with only a slight increase of the surface area.

Finally, the sample obtained at 200 °C preserves a high pore volume (0.77 $mL\,g^{-1}$), but the surface area is decreased by a factor of 4.2, from 525 to 125 $m^2\,g^{-1}$. This drastic decrease of the surface area is consistent with the completion of a full crystallisation process, which is also unambiguously highlighted by several factors: 1) the appearance of the β-AlF_3 phase revealed by the XRD pattern (Figure 1), 2) the strong increase of the fluorine content (Table 2), 3) the disappearance of organic moieties revealed by the very low carbon content (C% = 0.1 wt%) and 4) a strong increase of the internal pressure, from 20 to 50 bar. The last two features suggest that between 180 and 200 °C, the decomposition of the organic constituents takes place thanks to the high energy brought to the system. The strong increase of the internal pressure is indicative of a decomposition reaction. It has already been reported that microwave irradiation is able to induce side reactions: decomposition of organics molecules,[10] redox processes[5] and decomposition of ionic liquids.[11] The reaction mixture also contained some diethyl ether molecules as solvent, which are considered as inert under microwave irradiation since they are non-polar. Therefore, it can be assumed that diethyl ether molecules are not decomposed under microwave irradiation. Additionally, during the microwave synthesis of oxides, K. J. Rao et al.[12] reported the formation of diethyl ether molecules by condensation of alcohol molecules. Moreover, MS-coupled DTA/TG-investigations on the dry aluminium alkoxy fluoride clearly showed the formation of diethyl ether and water as result of Lewis acid (Al^{3+}) induced alcohol condensation.[9] Hence, it is considered likely that such a mechanism occurs here too: $2R\text{-}OH \rightarrow R\text{-}O\text{-}R + H_2O$. The released water can thus favour the hydrolysis of the alkoxy fluoride species as follows: $AlF_{3-x}(OiPr)_x + x\,H_2O \rightarrow AlF_{3-x}(OH)_x + x\,i$PrOH. The kinetics of fluorination can thus be improved by the decrease of steric hindrance induced by alkoxy ligands. Taking into account the already mentioned MS-coupled thermal investigations,[9] an alternative reaction path can be discussed. In this investigation, most of the solvated isopropanol molecules were desorbed between 100 and 150 °C; then the formation of propene as well as a very small amount of diethyl ether was detected between 175 and

225 °C. Consequently, in this temperature range a fluorinating gas must be provided to complete the fluorination. This conclusion is in full agreement with the synthesis procedure. By analogy with the thermal decomposition mechanism of the aluminium alkoxy fluoride, the process inducing the transformation of an amorphous phase into crystalline fluorides from microwave heating can be described as follows: 1) the increase of the synthesis temperature up to 180 °C favours the fluorination of the already formed aluminium alkoxy fluorides; thermal motions induced by the microwave irradiation increase the reactivity of fluoride anions toward the alkoxy group substitution; 2) at temperatures above 180 °C, breaking of the Al-O*i*Pr bonds can be considered to occur. In this scheme, bonds are cleaved forming propene and OH groups, as previously reported:[9] $Al{-}O{-}CH(CH_3)_2 \rightarrow Al{-}OH + CH_2{=}CH{-}CH_3$. This scheme is in good agreement with the drastic increase of the internal pressure occurring between heat treatments performed at 180 and 200 °C. The textural properties of the solid obtained at 200 °C exhibit a large pore size (50 nm in Table 1), which is consistent with the decomposition reaction that occurs. Additionally, after cooling down to room temperature, an internal pressure still remains inside the vessel, suggesting the presence of a gas phase.

Another remarkable point is that the decomposition of solvent molecules occurring between 180 and 200 °C induces a dissolution/recrystallisation process, leading to the metastable phase β-AlF_3 and the disappearance of the thermodynamically stable phase α-AlF_3. This reaction could be compared with the synthesis of nano-structured aluminium hydroxy fluorides by using microwave irradiation of a solution containing nitrate as the aluminium precursor in alcohol.[5] During such a synthesis an exothermic phenomenon occurs, involving the reduction of the nitrate precursor into ammonium species coupled with the oxidation of isopropanol. In this case also, the synthesis of the metastable beta phase implies a side reaction, which, finally, through drastic variation of the thermodynamic state (P, T), provides the required energy for the stabilisation of such a metastable β-form.

High-surface-area AlF_3 and acidic properties

Post-fluorination treatment using F_2 gas: It has been shown above that the microwave-assisted sol–gel synthesis leads to fluoride materials exhibiting a high-surface-area (above 500 $m^2 g^{-1}$). However, such a material still contains large numbers of organic moieties, since the carbon content is still around 12 wt% after microwave treatment at 180 °C (Table 2). To remove these species while retaining the high-surface-area, a low-temperature fluorination was performed with gaseous F_2. The sample obtained at 180 °C was selected because of its high-surface-area of up to 525 $m^2 g^{-1}$. To avoid a full crystallisation process, a medium temperature (225 °C) was chosen for the fluorination.

This post-fluorinated sample still exhibits a high-surface-area 330 $m^2 g^{-1}$, providing a suitable material for catalytic ability. It should be noted that the decrease of the surface area occurs along with a slight increase of both the pore size (8.5 nm) and the porous volume (0.87 $mL g^{-1}$) ascribed to the substitution of fluorine species for alkoxy groups. All the carbon atoms were removed, showing that the post-fluorination treatment enables the complete removal of organic moieties. No significant change was observed by X-ray diffraction analysis except for the detection of a peak located at 9.4 Å and noted with a sign "+" in Figure 3. The broad

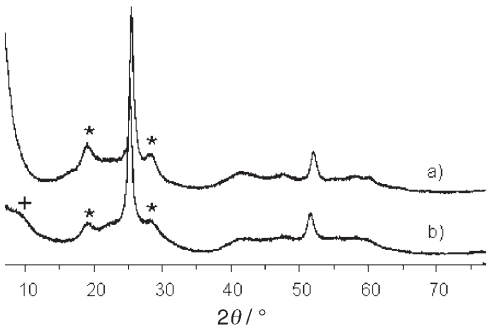

Figure 3. X-ray diffraction powder pattern of samples, a) microwave treated at 180 °C and b) after fluorination with undiluted F_2 gas at 225 °C (* unknown phase, + shoulder at 9.4 Å).

peaks located at around 4.7 and 3.1 Å are still present (asterisks in Figure 3). It should be noted that these three peaks can be indexed as multiples of reticular planes with $d = 9.4$ Å.

Figure 4 displays some TEM images of the F_2-treated sample. The solid consists of agglomerates built from large and small particles, denoted 1 and 2 in Figure 4A, respectively. Some of these large particles (50 nm) are displayed in Figure 4B. A zoom on a particle with a rodlike structure, 50 nm in length, shows interplanar distances of approximately 3.5–3.7 Å (insert in Figure 4B), which correspond to (012) inter-reticular distances of α-AlF_3. These large particles can therefore be ascribed to α-AlF_3 in agreement with the narrow FWHM of their X-ray peaks. The second type of particle, consisting of small crystalline domains of about 10 nm or less, are shown in Figure 4C. These domains present some interplanar distances of about 3 Å (Inset, Figure 4C). Such a distance is very close to the X-ray peak detected at 3.1 Å, which, in turn, is considered to characterise this phase. According to the high-surface-area of the solid, it is clear that these small particles of around 10 nm should be preponderant in the material.

Surface acidic properties: The surface acidic properties of this new high-surface-area aluminium fluoride (330 $m^2 g^{-1}$) have been investigated by catalytic tests and adsorption of pyridine by means of FT-IR spectroscopy.

First, catalytic tests were performed regarding the catalytic activity upon the $CHClF_2$ dismutation reaction. According to the data given in Table 3, the full catalytic activity of $CHClF_2$ dismutation proceeds after an activation period at 200 °C. This inductive period is required to remove water

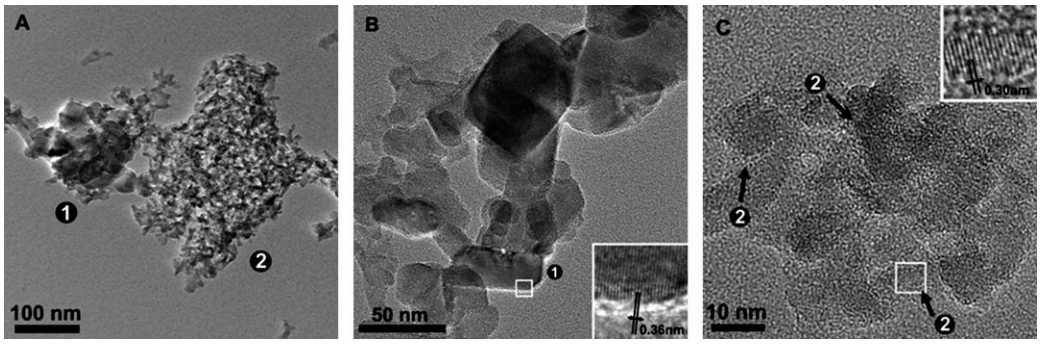

Figure 4. A) Transmission electron micrograph, B) and C) HRTEM image of high-surface-area aluminium fluoride.

Table 3. Catalytic activities of post-fluorinated high-surface-area AlF_3 ($330\ m^2g^{-1}$) sample toward the dismutation reaction of $CHClF_2$ and the isomerisation of 1,2-dibromohexafluoropropane (1,2-DBP).

	$CHClF_2$ dismutation						1,2-DBP isomerisation
T [°C]	100	150	200	150	100	50	
conversion rate [%]	2	2	97–98	≈100	≈100	≈100	18

molecules adsorbed on the surface. Once the catalyst is active, the dismutation reaction proceeds to completion even at 50 °C, showing high catalytic properties.

The isomerisation of 1,2-dibromohexafluoropropane has also been tested. This reaction is a good indicator of the presence of very strong Lewis acid sites, since it takes place only in presence of the strongest Lewis acids (amorphous HS-AlF_3, SbF_5, aluminium chloro fluoride). The rate of conversion is found to be 18 % and accounts for the presence of strong Lewis acid sites.

The type of surface acidic sites (Lewis or Brønsted) and their number have been determined by using pyridine (Py) adsorption at room temperature. The high-surface AlF_3 sample was outgassed at 300 °C prior to pyridine adsorption at room temperature. The spectrum obtained after introduction of 1 torr of pyridine and followed by evacuation at room temperature is shown in Figure 5. The 1400–1800 cm^{-1} range displayed contains typical vibration modes of coordinated pyridine. It is concluded that only Lewis acid sites are detected, since no band due to pyridine protonation (Brønsted acid site) was detected. Pyridinium species are indeed characterised by bands occurring around 1540 and 1640 cm^{-1}.

The wavenumber of the two bands at 1619 and 1453 cm^{-1} (ν8a and ν19b modes, respectively, of coordinated Py species) accounts for the strength of the Lewis acid sites,[13] that

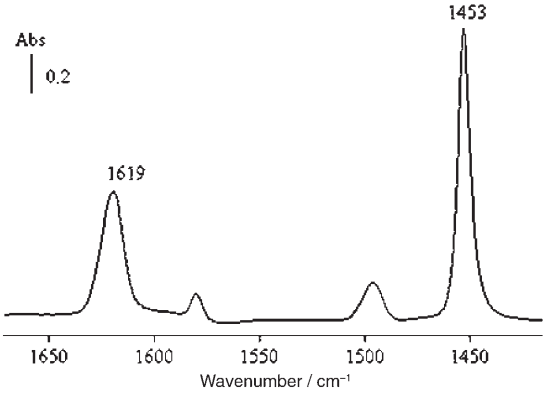

Figure 5. IR spectrum recorded after introduction of 1 torr of pyridine at room temperature on high-surface-area AlF_3 after outgassing at 300 °C followed by evacuation at room temperature.

is, the higher the wavenumber, the stronger the Lewis acidity. They are close to those previously reported for the β-AlF_3 compound,[14] and higher than those characterising the Lewis acidity of alumina[15] (1614 and 1448 cm^{-1}). Pyridine desorption at a higher temperature increases the ν8a and ν19b wavenumbers (Table 4). This phenomenon can be explained either by the site heterogeneity, by the weakest sites being liberated first, or by the pyridine inductive effects, which depend on the amount of adsorbed pyridine. The concentration of Lewis acid sites, estimated from the integrated

Table 4. Strength and concentration of Lewis acid sites detected by pyridine adsorption on fluorinated materials and alumina. F samples and alumina were pre-treated under vacuum at 300 and 500 °C, respectively.

	Outgassing temperature	HS AlF_3 ($330\ m^2g^{-1}$)	LS β-AlF_3 ($20\ m^2g^{-1}$)	HS β-AlF_3 ($82\ m^2g^{-1}$)	Pyrochlore ($130\ m^2g^{-1}$)	α-AlF_3 ($60\ m^2g^{-1}$)	γ-Alumina ($290\ m^2g^{-1}$)
19b band wavenumbers [cm^{-1}]	RT	1453	1454	1453.5	1451.5	1453	1448
	200 °C	1455.5	1455	1455	1454.5	1455	1454
	300 °C	1456	1456.5	1457	1456	1456	1455
Site numbers [$\mu mol\,g^{-1}$]	RT	615	35	200	336	158	480
	200 °C	283	20	100	137	63	110
	300 °C	203	10	43	77	32	40
Site numbers [per nm^2][a]	RT	1.12	1.05	1.47	1.56	1.59	1.00
	200 °C	0.52	0.60	0.73	0.63	0.63	0.23
	300 °C	0.37	0.30	0.32	0.36	0.32	0.08

[a] Estimated standard deviation: 6 %.

area of the ν19b band assuming a molar absorption coefficient value of 1.8 cm μmol^{-1},[14] is equal to about 615 μmol g^{-1}, or 1.1 site nm^{-2}.

It was important to compare the strength and the number of strong Lewis acid sites determined for this high-surface-area AlF_3 sample to those measured for other divided AlF_3 materials. Table 4 reports the strength and number of Lewis acid sites determined as reported above from the wavenumber and the intensity of the ν19b band after pyridine desorption at RT, 200, and 300 °C. The quoted AlF_3 materials are: 1) the post-fluorinated sample exhibiting a high-surface-area (330 m^2 g^{-1}) and therefore denoted HS-AlF_3, 2) two HTB samples with different surface areas[14,5] (20 and 82 m^2 g^{-1}) denoted LS (low surface area) and HS (high surface area) β-AlF_3, respectively, 3) a hydroxy fluoride exhibiting the pyrochlore type-structure[16] (130 m^2 g^{-1}) and 4) a derived form of α-AlF_3 (60 m^2 g^{-1}).[17]

As far as the AlF_3 samples are concerned, the signal for the ν19b band after pyridine outgassing at RT is shifted to a slightly lower wavenumber in the case of the pyrochlore sample. This can be related to the low fluorine content (F/Al = 1.8) of this material by comparison with the other compounds (F/Al > 2.5). The inductive effect of fluoride ions is also evidenced by the position of the ν19b band of γ-Al_2O_3, which possesses weaker Lewis acid sites than fluorinated materials.[16]

After pyridine desorption at 300 °C, the position of the ν19b band of the residual adsorbed species is similar whatever the sample, showing that the Lewis acid sites present similar strengths. This point should be regarded carefully and specified by adsorption of other probes like CO, which enables the discrimination between Lewis sites with different acid strengths.

The thermodesorption performed at 300 °C characterises the strongest Lewis acid sites. The ratio between the number of sites measured after thermodesorption at 300 °C and those measured after evacuation at RT enables the quantification of the proportion of strong Lewis acid sites exhibited by each solid. The highest proportion of strong Lewis acid sites is found on the HS-AlF_3 material, with 33 % of the Lewis acid sites being strong. This result suggests the occurrence of more homogeneous Lewis acid sites on the HS-AlF_3 material than on the other materials. In agreement with the promoting effect of fluoride ions, γ-alumina possesses the lowest fraction of strong Lewis acid sites, just 8 % of the total number of sites.

The most interesting result presented in Table 4 relates to the concentrations of Lewis acid sites per gram of material. They are much higher on HS-AlF_3 whatever the temperature of pyridine evacuation. Figure 6 clearly shows that the number of Lewis acid sites is correlated to the specific area.

This is the first time that such a correlation has been exemplified. This result underlines the interest of probe molecules adsorption/desorption experiments for characterising the number and strength of Lewis acidic sites in highly divided fluorine-based materials. Finally, it is worth noting that the number of strongest Lewis acid sites (Py outgassed at 300 °C) does not depend on the origin of the AlF_3 samples, as illustrated in the case of the pyrochlore sample. The latter indeed exhibits a large number of Lewis acid sites after thermodesorption at 300 °C. This fact can be rationalised by considering the finite size effect. The increase of the surface area is basically related to a decrease of the particle sizes. Chaudhuri et al.[18] have clearly shown that a decrease of the particle size was correlated with an increase of the number of under-coordinated Al^{3+} ions, that is, potential strong Lewis acid sites. Surface reconstruction taking into account the nanometric scale led to five- and even fourfold coordinated Al^{3+} ions, which should be regarded as very strong Lewis acid sites. This is consistent with our results, in which we find that the number of strong Lewis acid sites is related to the surface area, that is, to the particle size.

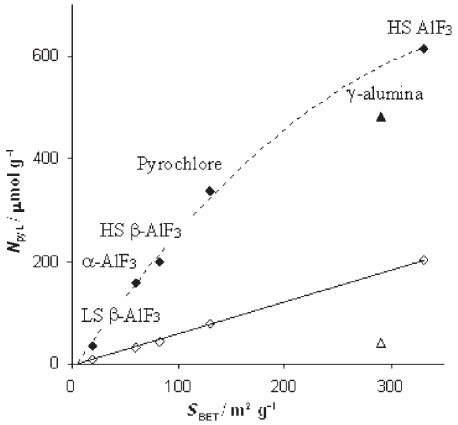

Figure 6. Dependence of the concentration of Lewis acid sites detected by pyridine adsorption on the specific area. Filled symbols: pyridine outgassed at room temperature; empty symbol: pyridine outgassed at 300 °C.

Conclusion

This work was based on the combination of two synthesis methods in which non-aqueous sol–gel fluoride material was further subjected to microwave irradiation. The crystalline state of the final material depends on the microwave-temperature treatment. An amorphous product is achieved at 90 °C and a crystalline phase exhibiting the HTB type structure at 200 °C. The mechanism of the amorphous⇄crystalline transformation of the gel under microwave irradiation has been discussed. It has been suggested that the decomposition of the gel induces the crystallisation process of the HTB phase.

In addition to a high-surface-area β-AlF_3, (125 m^2 g^{-1}), a multi-component material exhibiting a huge surface area of 525 m^2 g^{-1} has been prepared. This material contains residual organic moieties that were completely removed by low-temperature fluorination by using F_2 gas. This technique allows preservation of a surface area as high as 330 m^2 g^{-1}. From HRTEM experiments this material is shown to be built of two types of nano-particles: 50 nm crystallites ascri-

bed to α-AlF_3, and smaller particles of about 10 nm related to an unidentified phase.

This work has also confirmed that the microwave-assisted synthesis is a suitable route to achieve high-surface-area materials. This method is a fast and simple procedure that could be easily applied to the synthesis of other high-surface-area metal fluorides. It opens a promising way to develop more divided materials and stabilise novel phases. Since the interaction between the microwaves and the mixture is a decisive step on the final stabilised material, further work should be performed incorporating different organic solvents such as butanol or ionic liquids to tune the reactivity and the behaviour of the mixture under microwave irradiation. The ability of solvents to generate heat under microwave irradiation could be one way to obtain new aluminium-based fluoride frameworks, as well as highly divided materials.

FT-IR spectroscopy on Al-based fluorides materials shows for the first time that the number of strong Lewis acid sites is primarily related to the surface area, whatever the structure/composition of the compound. This result highlights the role of surface reconstruction occurring on a nanoscopic scale leading to the formation of the strongest Lewis acid sites.

Acknowledgement

The EU is gratefully acknowledged for financial support through the 6th Framework Programme (FUNFLUOS, Contract No. NMP3-CT-2004–5005575).

[1] E. Kemnitz, U. Groß, S. Rudiger, C. S. Shekar, *Angew. Chem.* **2003**, *115*, 4383; *Angew. Chem. Int. Ed.* **2003**, *42*, 4251.
[2] S. Rudiger, G. Eltanany, U. Groß, E. Kemnitz, *J. Sol–gel Sci. Technol.* **2007**, *41*, 299.
[3] C. O. Kappe, *Angew. Chem.* **2004**, *116*, 6408; *Angew. Chem. Int. Ed.* **2004**, *43*, 6250.
[4] D. Adam, *Nature* **2003**, *421*, 571.
[5] D. Dambournet, A. Demourgues, C. Martineau, S. Pechev, J. Lhoste, J. Majimel, A. Vimont, J.-C. Lavalley, C. Legein, J-Y. Buzaré, F. Fayon, A. Tressaud, *Chem. Mat.* **2008**, *20*, 1459
[6] P. Daniel, A. Bulou, M. Rousseau, J. Nouet, J. L Fourquet, M. Leblanc, R. Burriel, *J. Phys. Condens. Matter* **1990**, 5663.
[7] A. Kutoglu, *Z. Kristallogr.* **1992**, *199*, 197.
[8] A. Le Bail, C. Jacoboni, M. Leblanc, R. De Pape, H. Duroy, J. L. Fourquet, *J. Solid State Chem.* **1988**, *77*, 96.
[9] S. Ruediger, U. Groß, M. Feist, H. A. Prescott, S. Chandra Shekar, S. I. Troyanov, E. Kemnitz, *J. Mater. Chem.* **2005**, *15*, 588.
[10] I. V. Kubrakova, R. Kh. Khamizov, *Russ. Chem. Bull.* **2005**, *54*, 1413.
[11] D. S. Jacob, L. Bitton, J. Grinblat, I. Felner, Y. Koltypin, A. Gedanken, *Chem. Mater.* **2006**, *18*, 3162.
[12] K. J. Rao, K. Mahesh, S. Kumar, *Bull. Mater. Sci.* **2005**, *28*, 19.
[13] G. Busca, *Phys. Chem. Chem. Phys.* **1999**, *1*, 723.
[14] A. Vimont, J. C. Lavalley, L. Francke, A. Demourgues, A. Tressaud, M. Daturi, *J. Phys. Chem. B* **2004**, *108*, 3246–3255.
[15] A. Vimont, J. C. Lavalley, A. Sahibed-Dine, C. Otero Arean, M. Rodriguez Delgado, M. Daturi, *J. Phys. Chem. B* **2005**, *109*, 9656.
[16] D. Dambournet, A. Demourgues, C. Martineau, E. Durand, J. Majimel, A. Vimont, H. Leclerc, J-C. Lavalley, M. Daturi, C. Legein, J.-Y. Buzaré, F. Fayon, A. Tressaud, *J. Mater. Chem.*, **2008**, DOI: 10.1039/B718856K.
[17] D. Dambournet, A. Demourgues,C. Martineau, E. Durand, J. Majimel, C. Legein, J-Y. Buzaré, F. Fayon, M. Daturi, A. Tressaud, unpublished results.
[18] S. Chaudhuri, P. Chupas, B. J. Morgan, P. A. Madden, C. P. Grey, *Phys. Chem. Chem. Phys.* **2006**, *8*, 5045.

Received: November 21, 2007
Revised: January 28, 2008
Published online: May 19, 2008

